# Resistance of human glioblastoma multiforme cells to growth factor inhibitors is overcome by blockade of inhibitor of apoptosis proteins

David S. Ziegler,[1] Renee D. Wright,[1] Santosh Kesari,[2] Madeleine E. Lemieux,[1] Mary A. Tran,[3] Monish Jain,[3] Leigh Zawel,[3] and Andrew L. Kung[1]

[1]Department of Pediatric Oncology, Dana-Farber Cancer Institute and Children's Hospital Boston, Harvard Medical School, Boston, Massachusetts, USA. [2]Department of Medical Oncology and Department of Cancer Biology, Dana-Farber Cancer Institute, and Department of Neurology, Brigham and Women's Hospital, Harvard Medical School, Boston, Massachusetts, USA. [3]Novartis Institutes for BioMedical Research, Cambridge, Massachusetts, USA.

**Multiple receptor tyrosine kinases (RTKs), including PDGFR, have been validated as therapeutic targets in glioblastoma multiforme (GBM), yet inhibitors of RTKs have had limited clinical success. As various antiapoptotic mechanisms render GBM cells resistant to chemo- and radiotherapy, we hypothesized that these antiapoptotic mechanisms also confer resistance to RTK inhibition. We found that in vitro inhibition of PDGFR in human GBM cells initiated the intrinsic pathway of apoptosis, as evidenced by mitochondrial outer membrane permeabilization, but downstream caspase activation was blocked by inhibitor of apoptosis proteins (IAPs). Consistent with this, inhibition of PDGFR combined with small molecule inactivation of IAPs induced apoptosis in human GBM cells in vitro and had synergistic antitumor effects in orthotopic mouse models of GBM and in primary human GBM neurospheres. These results demonstrate that concomitant inhibition of IAPs can overcome resistance to RTK inhibitors in human malignant GBM cells, and suggest that blockade of IAPs has the potential to improve treatment outcomes in patients with GBM.**

## Introduction

The treatment of malignant gliomas remains one of the greatest challenges facing adult and pediatric oncologists today. At the most severe end of the spectrum is glioblastoma multiforme (GBM), one of the most malignant of cancers, with a median survival of less than 12 months and an inherent resistance to both chemo- and radiotherapeutics (1). While initial treatment of GBM with surgery, radiotherapy, and chemotherapy often produces some palliation of symptoms, these tumors almost universally recur with an unrelenting progression to death. Despite great advances in our understanding of the molecular causes of GBM (2), there has been very little improvement in outcomes for patients with GBM.

A variety of growth factor receptors are instrumental in the tumorigenesis of gliomas and have been validated as therapeutic targets. EGFR amplification is the most common genetic abnormality in adult high-grade gliomas, and EGFR overexpression has been demonstrated in up to 85% of cases (3). Glioblastomas also often express EGFRvIII, a genomic deletion variant of EGFR that is constitutively active (4). Similarly, IGF-1 receptor (IGF-1R) has been shown to be abnormally active in gliomas (5), and its inhibition prevents tumor growth in preclinical models (6). Malignant gliomas also often exhibit overexpression of both PDGF and PDGFR, which contribute to tumor progression via an autocrine or paracrine loop (7–9). Antagonism of PDGFR with the tyrosine kinase inhibitor imatinib (also known as STI571 and Gleevec) in both in vitro and in vivo glioma models has demonstrated successful inhibition of tumor growth (10).

The promising laboratory results seen with receptor tyrosine kinase (RTK) inhibitors in gliomas have thus far not translated into clinical success. Initial reports of the use of imatinib in patients with recurrent malignant gliomas reveal limited single-agent activity with few responders and a 6-month progression-free survival of only 3% (11). Only 10%–20% of patients have a clinical response to EGFR kinase inhibitors, and most responders subsequently exhibit rapid tumor progression (12, 13).

The mechanisms of resistance to RTK inhibition have not been fully elucidated (14). Tumor cells unresponsive to EGFR inhibitors are characterized by reduced induction of apoptosis (15). Furthermore, while imatinib dramatically increases apoptosis in BCR-ABL–positive chronic myelogenous leukemia and in gastrointestinal stromal tumors, it does not induce apoptosis when administered to glioblastoma cells either in vitro or in vivo, even at high concentrations (10, 16). Multiple antiapoptotic mechanisms are known to be activated in glioma cells (17–19). Mutation of the PTEN tumor suppressor results in activation of the PI3K/AKT pathway, which provides key antiapoptotic signals (3, 20). The proapoptotic activities of p53 are often lost due to mutation or overexpression of MDM2 (3, 21). Multiple members of the BCL2 family are dysregulated (22). The inhibitor of apoptosis proteins (IAPs) represent the final molecular blockade preventing apoptosis by inhibiting the activity of caspase-3, -7, and -9. IAPs have been shown to be highly expressed in malignant gliomas (23, 24). The IAP survivin has been identified in the majority of malignant gliomas, where its levels correlate inversely with prognosis (25). Peptides that inhibit IAPs have been shown to synergize with TNF-related apoptosis-inducing ligand (TRAIL) and to enhance apoptosis in glioma cells both in vitro and in vivo (26–28).

**Nonstandard abbreviations used:** BBB, blood-brain barrier; GBM, glioblastoma multiforme; IAP, inhibitor of apoptosis protein; IGF-1R, IGF-1 receptor; MOMP, mitochondrial outer membrane permeabilization; NOL3, nucleolar protein 3; RTK, receptor tyrosine kinase.

**Conflict of interest:** The authors have declared that no conflict of interest exists.

**Citation for this article:** *J. Clin. Invest.* **118**:3109–3122 (2008). doi:10.1172/JCI34120.

We hypothesized that the antiapoptotic mechanisms that render glioma cells resistant to cytotoxic agents (chemotherapy and radiotherapy) may also modulate their response to targeted therapies such as RTK inhibitors. In this study, we demonstrate that inhibition of PDGFR with imatinib results in activation of the apoptotic cascade, but downstream blockade of caspase activation prevents apoptosis. We show that the apoptosis repressor with CARD domain (ARC, also known as and referred to heareafter as nucleolar protein 3 [NOL3]) antiapoptotic protein may play a role in gliomas and is modulated by imatinib. We show that inhibition of the IAPs with LBW242, a small molecule that binds to and inhibits the BIR3 domain of IAPs, produces full-blown apoptosis in combination with PDGFR inhibition and results in synergistic antitumor efficacy in vitro and in vivo. These results suggest a potential strategy for increasing the clinical efficacy of RTK inhibitors in patients with gliomas and perhaps other malignancies.

## Results

*Inhibition of IAPs with LBW242*. It has been proposed that cancer cells exist in a state of dynamic tension with a constant burden of proapoptotic signals counterbalanced by heightened expression of antiapoptotic proteins (29). The IAPs constitute a final blockade of apoptosis through sequestration of caspase-3, -7, and -9 (Figure 1A). Upon mitochondrial permeabilization, release of Smac/DIABLO into the cytoplasm results in binding to, and inactivation of, IAPs. Since IAPs are overexpressed in gliomas (23–25), it is possible that blockade of IAPs alone may be sufficient to shift the balance towards apoptosis in glioma cells. The small-molecule IAP inhibitor LBW242 (Figure 1A) was developed through iterative binding optimization and depeptidization of the aminoterminal 4 amino acids of Smac, which is necessary and sufficient for binding to the BIR3 domain of IAPs (30). To confirm that LBW242 does in fact effectively function as a Smac mimetic, we first performed a FRET-based competition assay that measured the ability of LBW242 to compete with Smac for binding to the BIR3 domain of XIAP. LBW242 inhibited the interaction of full-length Smac to XIAP in a well-behaved sigmoidal dose-response relationship. To confirm the functional significance of the binding of LBW242 to IAPs, we next assessed the effect of LBW242 binding on caspase activity in a cell-free system. In an assay in which the activity of caspase-9 was blocked by recombinant XIAP-BIR3, increasing doses of LBW242 resulted in caspase-9 activation with subsequent activation of caspase-3 and cleavage of a fluorogenic substrate (Figure 1C).

Because several previously reported peptide IAP inhibitors have been confounded by their limited cellular and tissue penetration in a variety of tumors (26, 31–33), we next assessed the effects of LBW242 in intact cells. LN827 glioma cells were exposed to LBW242 for 4 hours, and then endogenous caspase-9 was immunoprecipitated from whole cell extracts. Although LBW242 did not have any effect on the overall levels of caspase-9, or XIAP (Figure 1, D and E), the abundance of endogenous XIAP bound to caspase-9 was reduced in cells treated with LBW242 (Figure 1, D and F). These results establish the cellular permeability of LBW242 and the ability of LBW242 to disrupt endogenous binding of IAPs to caspase-9 in intact cells.

To determine the achievable tissue concentrations of LBW242 in the in vivo setting, we administered LBW242 parenterally to mice at a dose of 50 mg/kg/d. After 14 days of daily dosing, LBW242 achieved a long-term steady-state concentration that exceeded 60 μM in tumors (Figure 1G). For treatment of intracranial tumors, the blood-brain barrier (BBB) is an impediment to drug bioavailability. We found that LBW242 was able to cross even the intact BBB and achieve tissue concentrations of approximately 25 μM in normal brain (Figure 1G). The BBB is at least partially disrupted within brain tumors (34), suggesting that achievable brain tumor levels exceed 25 μM. Prior studies have demonstrated the ability of LBW242 to inhibit the growth of hematologic malignancy cell lines as a single agent with $IC_{50}$ values in the 10–30 μM range (30). We assessed the effect of LBW242 on glioma cell proliferation in vitro and found no stand-alone effects on the growth of U87 cells (Figure 1H) or LN827 cells (data not shown) up to concentrations of 50 μM. U87 (WT p53, mutant PTEN, p16 and p14 deleted) and LN827 (p53 hemizygous, mutant PTEN, p16 and p14 deleted) (21) glioma cell lines were selected for study because of their robust in vitro and orthotopic in vivo growth. U87 cells are further known to be dependent upon a PDGFR autocrine signaling loop (35). Since in vivo steady-state tissue levels of LBW242 exceed 25–60 μM, since there were no stand-alone effects on glioma growth up to 50 μM, and since caspase activity was most efficiently reversed in vitro at 50 μM concentrations, we used a standardized concentration of 50 μM for all subsequent combination studies.

*Effects of PDGFR and IAP inhibition on glioma cell growth*. Although IAP inhibition had no monotherapeutic activity, we hypothesized that apoptosis might be achieved by simultaneously increasing proapoptotic signals. Since PDGFR has a well-established role in gliomagenesis, and since withdrawal of growth factor signaling is proapoptotic in many systems (36), we assessed the combined effects of IAP and PDGFR inhibition on cell growth. As a single agent, imatinib inhibited cell growth at doses of 20 μM or more (Figure 2A). The addition of LBW242, which had no effect on cell growth alone, resulted in a shift in the imatinib dose-response curve toward increased sensitization in LN827 and U87 cells (Figure 2A). Over 4 days of treatment, only mild cytostasis is apparent with either imatinib or LBW242 alone, compared with frank cell death in cells treated with both agents (Figure 2B).

Since small molecule kinase inhibitors are not monospecific, we questioned whether the observed effects were mediated through inhibition of PDGFR or through off-target effects on other kinases. While treatment with imatinib had no effects on the overall abundance of PDGFR, the activation state of PDGFR was almost completely abolished by imatinib at 2.5 μM in LN827 cells (Figure 2C). When administered as monotherapy, inhibition of LN827 cell growth was observed at imatinib concentrations of 20 μM or more (Figure 2A). In contrast, the synergistic effect on cell growth when imatinib was combined with LBW242 was observed at imatinib concentrations of approximately 1.25–2.5 μM (Figure 2A). The correlation of dosages causing PDGFR inhibition and synergistic inhibition of tumor growth suggests that the response seen occurred as a result of PDGFR inhibition. LBW242 had no effect on PDGFR abundance or activity (Figure 2C), suggesting that the synergistic effects of the combination are not due to LBW242 potentiating the inhibitory effects of imatinib on PDGFR activation.

To further confirm that the synergy observed resulted from PDGFR inhibition, we also tested the combination of LBW242 with an alternative PDGFR kinase inhibitor AMN107 (nilotinib; Figure 2D) (37). A synergistic inhibition of cell growth was again apparent with the combination treatment. Similar results were also seen when LBW242 was tested in combination with the PDGFR inhibitor dasatinib (data not shown). Together, these

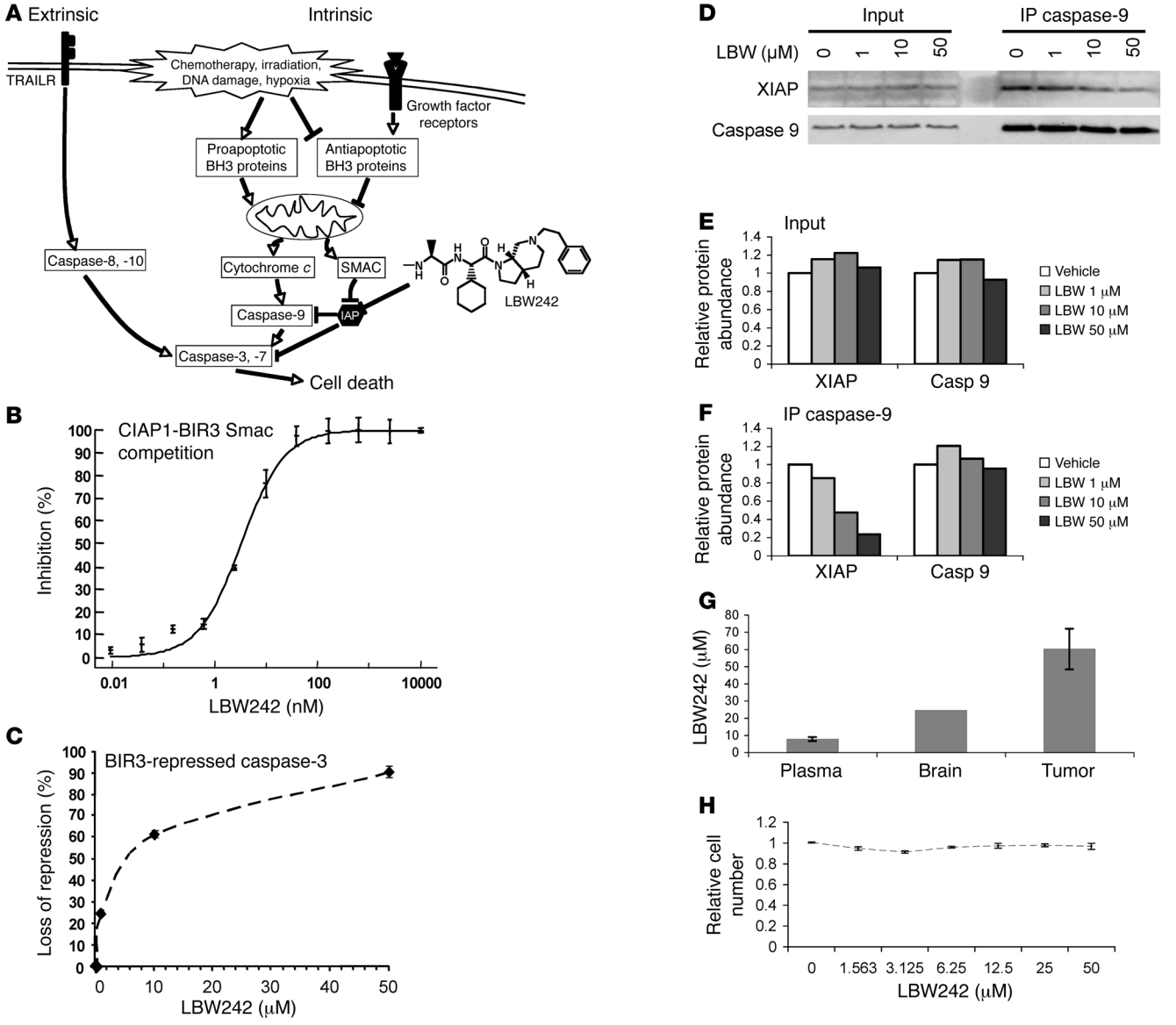


**Figure 1**

Structure and function of LBW242. (**A**) Schematic of the apoptotic pathway with structure and site of action of LBW242, which binds to the IAPs and prevents their neutralization of the caspases. (**B**) LBW242 competes with full-length Smac for occupancy of the XIAP-BIR3 surface groove, as assessed by a time-resolved fluorescence energy transfer assay. (**C**) LBW242 overcomes XIAP-BIR3–mediated repression of caspase-3 activity in a cell-free extract, resulting in activation of caspase-3 and cleavage of a fluorogenic substrate. (**D**) LN827 cells treated with the indicated concentrations of LBW242 for 4 hours reveal no change in cellular levels of XIAP or caspase-9 (input). Immunoprecipitation of caspase-9 followed by immunoblot analysis revealed dose-dependent decrease in associated XIAP (IP caspase-9). (**E** and **F**) Densitometric analysis with data expressed relative to vehicle controls. (**G**) LBW242 concentrations in plasma, brain, and tumor of 3 SK-OV-3 tumor–bearing nude mice after 14 days of daily parenteral dosing of LBW242 (50 mg/kg), measured 4 hours following the final dose. Data represent mean ± SEM for plasma and tumor, and the average of pooled samples for brain. (**H**) U87 cells were treated in triplicate with the indicated concentrations of LBW242. Relative cell numbers were assessed by 3-(4,5-dimethylthiazol-2-yl)-5-(3-carboxymethoxyphenyl)-2-(4-sulfophenyl)-2H-tetrazolium, inner salt (MTS) assay (see Methods). Data points represent the mean ± SEM.

results demonstrate that inhibition of IAPs in glioma cells has little stand-alone activity but synergizes with inhibition of PDGFR, which is known to play a key role in gliomagenesis. Stand-alone activity was observed with imatinib alone, but only at concentrations more than 10-fold above that required for PDGFR inhibition, suggesting that off-target inhibition of other kinases contributes to this single agent activity.

*Imatinib activates the intrinsic pathway, but apoptosis requires concomitant blockade of IAPs.* Given the established role for PDGFR in gliomas, and in light of the above results, we hypothesized that PDGFR inhibition may produce a proapoptotic signal that is counteracted by downstream antiapoptotic proteins. Multiple upstream proapoptotic signals converged at the level of the mitochondria, resulting in mitochondrial outer membrane per-

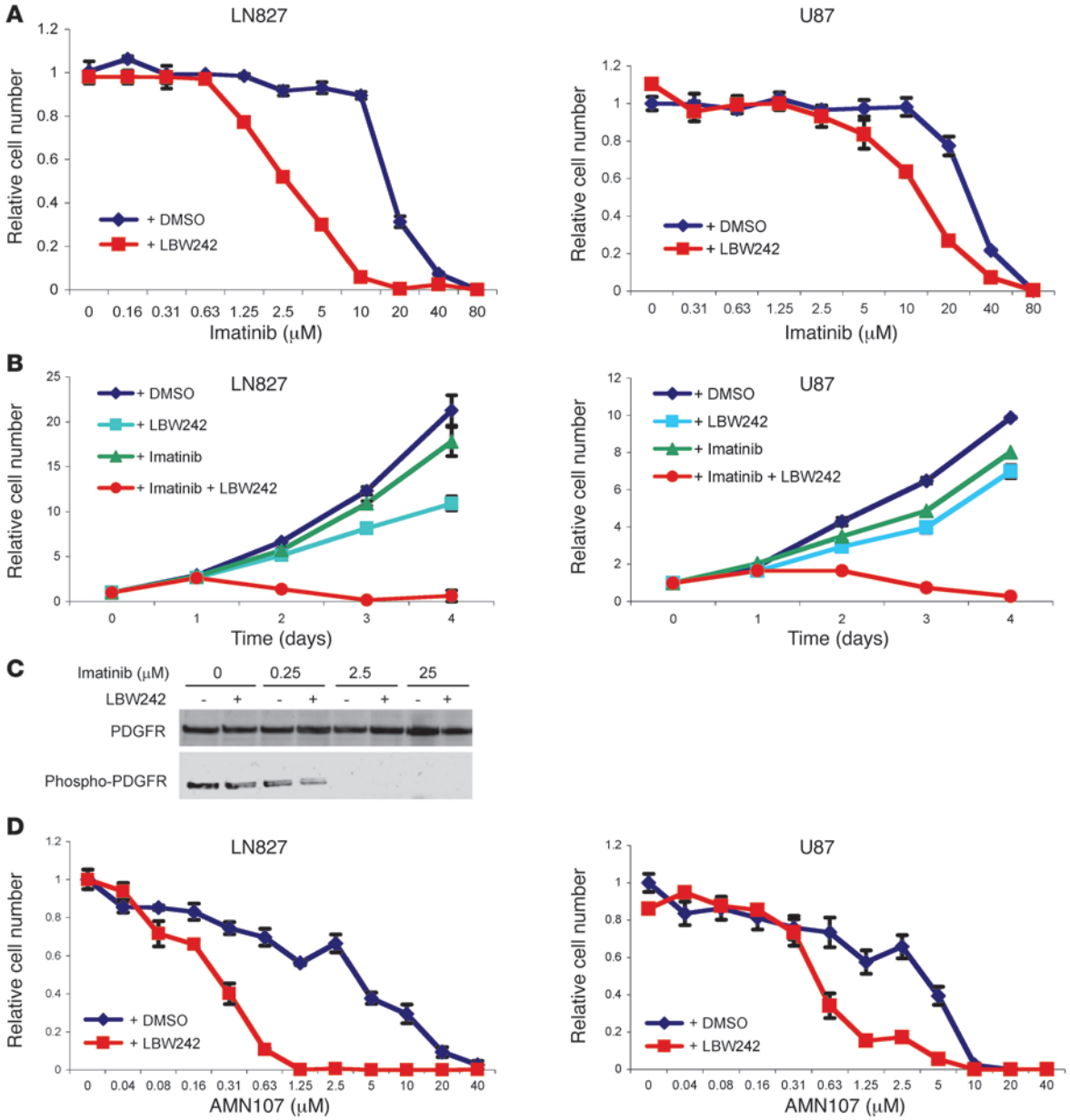


**Figure 2**

Synergistic effects of LBW242 and imatinib. (**A**) U87 and LN827 cells were treated with the indicated concentrations of imatinib in combination with LBW242 (50 μM) or DMSO control. Cell numbers were determined 72 hours later via MTS. Data are expressed as mean ± SEM of triplicates. Similar results were observed in >3 independent experiments. (**B**) U87 and LN827 cells were seeded in 96-well plates and treated with LBW242 (50 μM), imatinib (8 μM), LBW242 plus imatinib, or DMSO control. The number of viable cells was measured via MTS assay after 24, 48, 72, and 96 hours. The data are expressed relative to the first day of treatment and are represented as the mean ± SEM of triplicates. (**C**) Serum-starved LN827 cells were treated for 90 minutes with dosages of imatinib and LBW242 as indicated. Levels of PDGFR and phospho-PDGFR were measured following immunoprecipitation and immunoblotting. (**D**) U87 and LN827 cells were seeded in 96-well plates and treated with the PDGFR inhibitor AMN107 at the dosages indicated in combination with LBW242 (50 μM) or DMSO control. Cellular proliferation was measured via MTS assay after 72 hours of incubation. Data are represented as the mean ± SEM or triplicates.

meabilization (MOMP) and release of the proapoptotic mediators cytochrome *c* and Smac/DIABLO (Figure 1A). Therefore, we studied whether imatinib induced MOMP, by measuring the cytoplasmic levels of cytochrome *c* and Smac/DIABLO. In LN827 cells, imatinib at 10 μM, which had no effects on cell growth (Figure 2, A and B), led to a significant increase in both cytoplasmic cytochrome *c* and Smac/DIABLO (Figure 3A). Consistent with its mechanism of action, LBW242 had no appreciable effect on cytochrome *c* or Smac/DIABLO levels, either as a single agent or in combination with imatinib (Figure 3A). The concentration of imatinib at which MOMP was observed was 2.5 μM (Figure 3A), which coincided with the concentration at which PDGFR activ-

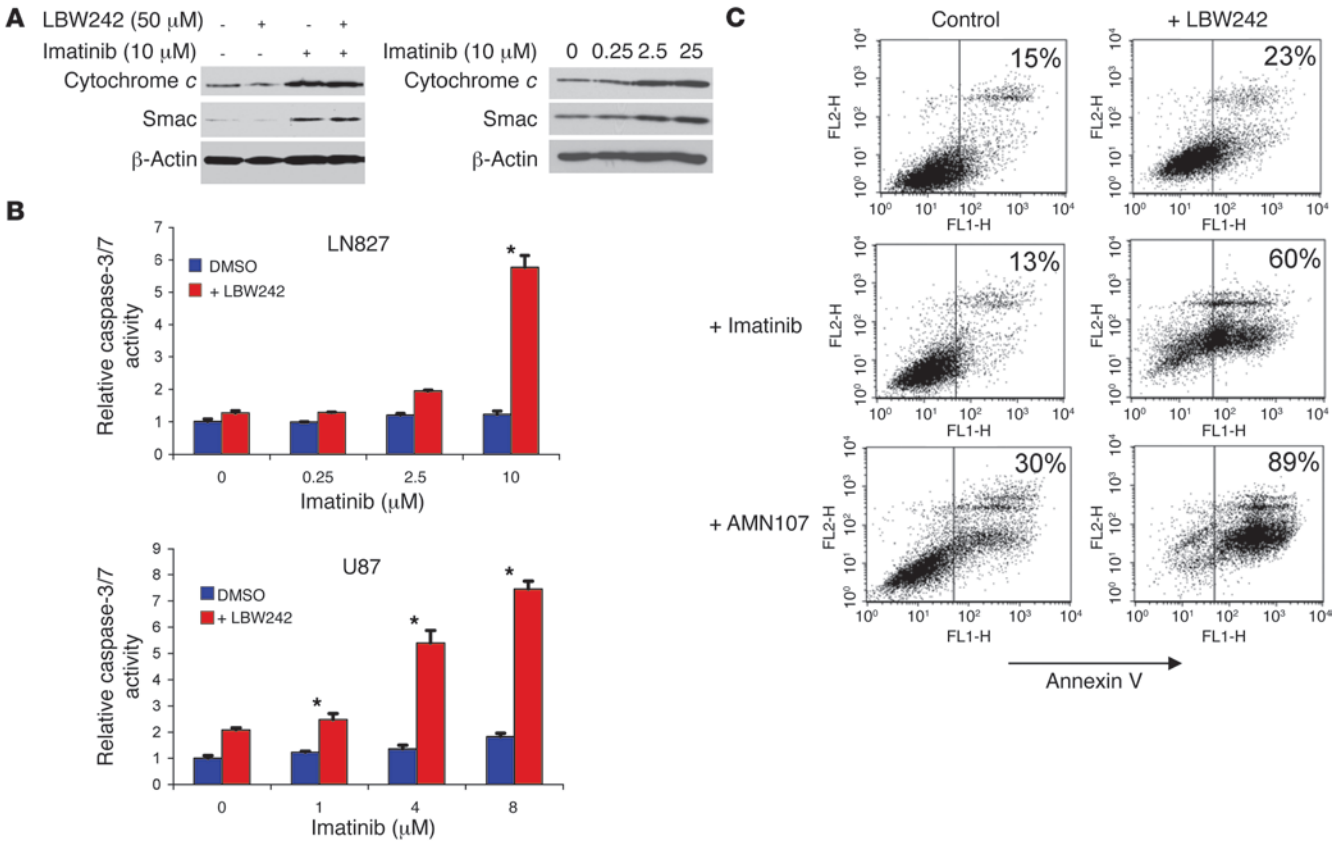


**Figure 3**

PDGFR and IAP inhibition combine to enhance caspase activity and activate apoptosis in glioma cells. (**A**) LN827 cells were treated with drugs as indicated for 48 hours, following which the cellular cytoplasm was separated from mitochondria. The cytosol was collected and subjected to immunoblotting for cytochrome *c* and Smac/DIABLO. (**B**) LN827 and U87 cells were treated with imatinib at the dosages indicated for 48 hours in combination with LBW242 (50 μM) or DMSO control. Caspase-3/7 activity is expressed relative to controls as mean ± SEM of triplicates. **P* < 0.01, 2-tailed Student's *t* test. (**C**) Apoptosis was measured as the proportion of cells staining positive for annexin V after 72 hours of incubation with LBW242 (50 μM) in combination with or without imatinib (10 μM) or AMN107 (5 μM). Cells to the left of the divider in each panel are negative for annexin V, and positive cells are to the right. The number in the upper right corners indicates the percentage of annexin V–positive cells in each treatment group. Similar results were obtained in 3 independent experiments.

ity was inhibited (Figure 2C) and where synergistic killing with LBW242 was observed (Figure 2A) in LN827 cells.

Although imatinib induced MOMP (Figure 3A), there was no activation of caspase-3 or -7 when cells were treated with imatinib alone (Figure 3B). The addition of LBW242 resulted in significant activation of caspase-3/7 activity (Figure 3B). To determine if the synergistic activation of caspase-3/7 activity resulted in apoptosis, we measured the number of cells staining positive with annexin V. PDGFR inhibition with imatinib alone and IAP inhibition with LBW242 alone caused minimal change over the basal level of apoptosis, but the combination of imatinib and LBW242 resulted in synergistic induction of apoptosis (Figure 3C). A small increase in apoptosis was apparent with AMN107 alone, but again the addition of LBW242 resulted in the majority of tumor cells undergoing apoptosis (Figure 3C).

Recent reports have suggested that IAP inhibitors regulate the activity of the extrinsic apoptotic pathway in certain tumor types (38–40). We therefore assessed the effect of imatinib with or without LBW242 on caspase-8 activity but found no significant changes (Supplemental Figure 1; supplemental material available online with this article; doi:10.1172/JCI34120DS1), suggesting that the mechanism of synergy is limited to the intrinsic pathway. Together, these results establish that imatinib activates the intrinsic apoptosis pathway and MOMP but that caspase-3 and -7 are not activated unless the IAPs are simultaneously blocked with LBW242. The combination of PDGFR and IAP inhibition produces synergistic induction of apoptosis.

*RTK and IAP inhibition activates caspases and suppresses tumor growth independently of Akt.* Several RTKs have been implicated in gliomagenesis, and we wondered whether the synergistic effects of PDGFR and IAP inhibition could be generalized to other growth factor receptors. First we assessed the combination of IAP inhibition and blockade of IGF-1R with NVP-AEW541, a highly specific IGF-1R kinase inhibitor (41). The combination of AEW541 and LBW242 led to caspase-3/7 activation and synergistically inhibited tumor cell growth (Supplemental Figure 2A). Next we tested blockade of EGFR with a dual EGFR and HER2 kinase inhibitor PKI166 (42). PKI166 as a single agent had a proapoptotic effect with increased levels of caspase-3/7 activation. However the addition of IAP inhibition led to enhanced caspase-3/7 activation and a correlative enhanced inhibition of glioma cell proliferation (Supplemental Figure 2B). It is known

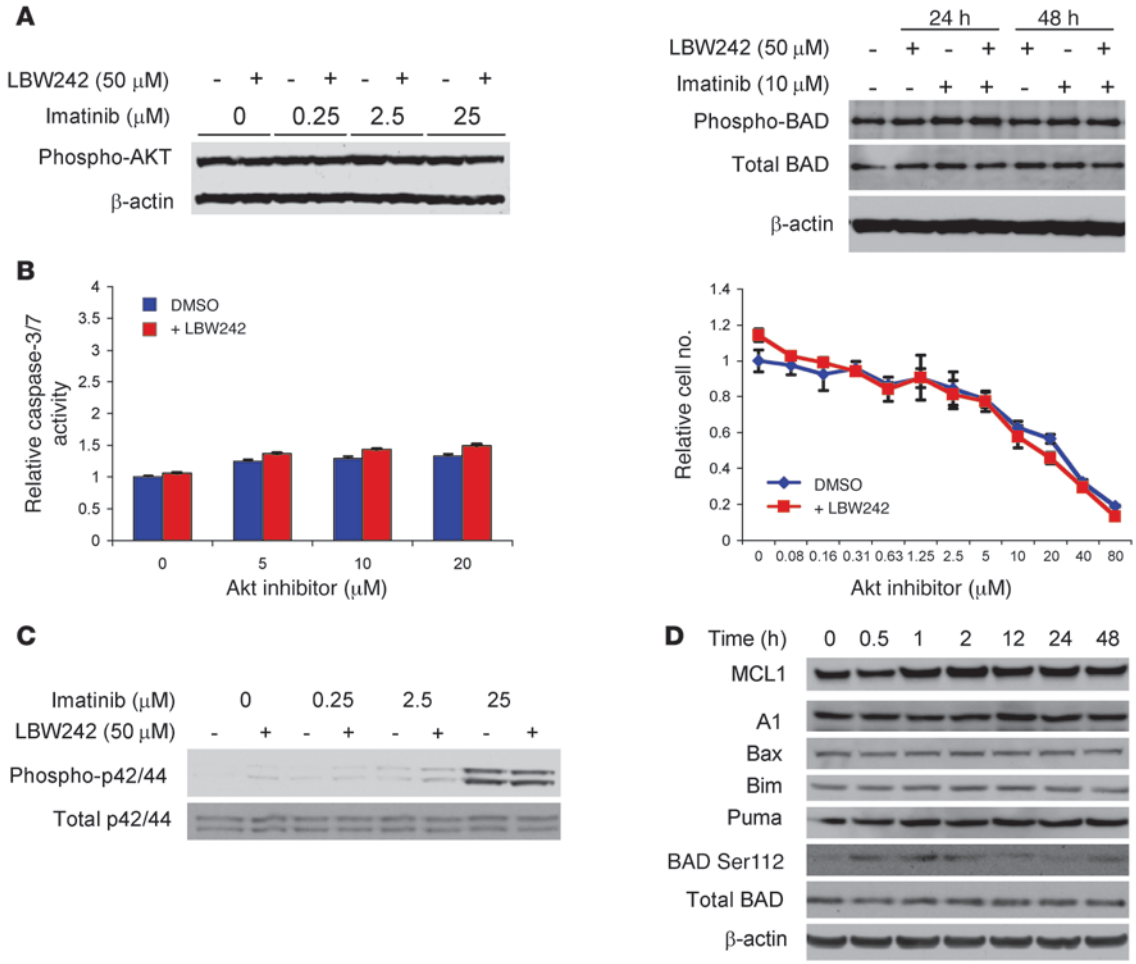


**Figure 4**
Imatinib induces apoptosis independent of Akt. (**A**) LN827 cells were treated with imatinib with or without LBW242, as indicated. No appreciable effects on Akt activation were apparent after 6 hours of treatment, as assessed by Ser473 phosphorylation. No effects on total or Ser112 phosphorylated BAD were apparent at 24 or 48 hours. (**B**) LN827 cells were treated with the Akt inhibitor triciribine at the dosages indicated and with LBW242 (50 μM) or DMSO. Caspase-3/7 activity was measured at 48 hours and total cell number at 72 hours. (**C**) Effects of imatinib with or without LBW242 on p42/44 activation were assessed after 6 hours. (**D**) Effects of imatinib with or without LBW242 on BCL2 family members were assessed at the indicated times. In all cases, no significant differences were apparent.

that glioma cells lose overexpression of EGFR in culture (21), which may explain the overall modest effects observed.

Because PDGFR, EGFR, and IGF-1R all activate Akt, and since Akt provides key antiapoptotic signals, we asked whether the demonstrated induction of apoptosis and inhibition of cell growth occur secondary to Akt inactivation. As shown in Figure 4A, Akt is tonically phosphorylated in LN827 cells. Administration of imatinib with or without LBW242 did not inhibit Akt phosphorylation, nor did it inhibit the downstream phosphorylation of BAD (Figure 4A). Furthermore, the combination of LBW242 and the specific Akt inhibitor triciribine did not demonstrate any notable synergistic effect on either caspase-3/7 activation or tumor cell proliferation (Figure 4B). Thus the synergy between growth factor inhibition and IAP inhibition appears to occur independently of Akt status. It should be noted that these studies were done in the presence of serum and in cells that are PTEN deficient (21), indicating only that Akt signaling is not attenuated under these conditions, not that PDGFR does not signal through Akt.

We next tested for alternative mechanisms by which PDGFR inhibition may lead to activation of the apoptotic pathway and MOMP. Because Erk 1/2 is another downstream target of growth factor receptors, we assessed its phosphorylation status and found that treatment with imatinib did not inhibit Erk 1/2 phosphorylation (Figure 4C). We also investigated whether treatment with imatinib led to a change in expression of a number of anti- or proapoptotic members of the BCL2 family of proteins. However, we were unable to detect any significant change in the broad range of proteins tested (Figure 4D).

To more comprehensively assess the effect of imatinib on a broad number of pro- and antiapoptotic mediators, we assessed mRNA expression using a 96-well quantitative RT-PCR microarray format as described previously (43). Treatment with imatinib 10 μM resulted in a significant change in the expression of only 1 gene tested — NOL3 (Supplemental Figure 3). Imatinib was found to decrease *NOL3* mRNA abundance in 7 individual multi-well screens. *NOL3* encodes the antiapoptotic protein ARC, which is known to be high-

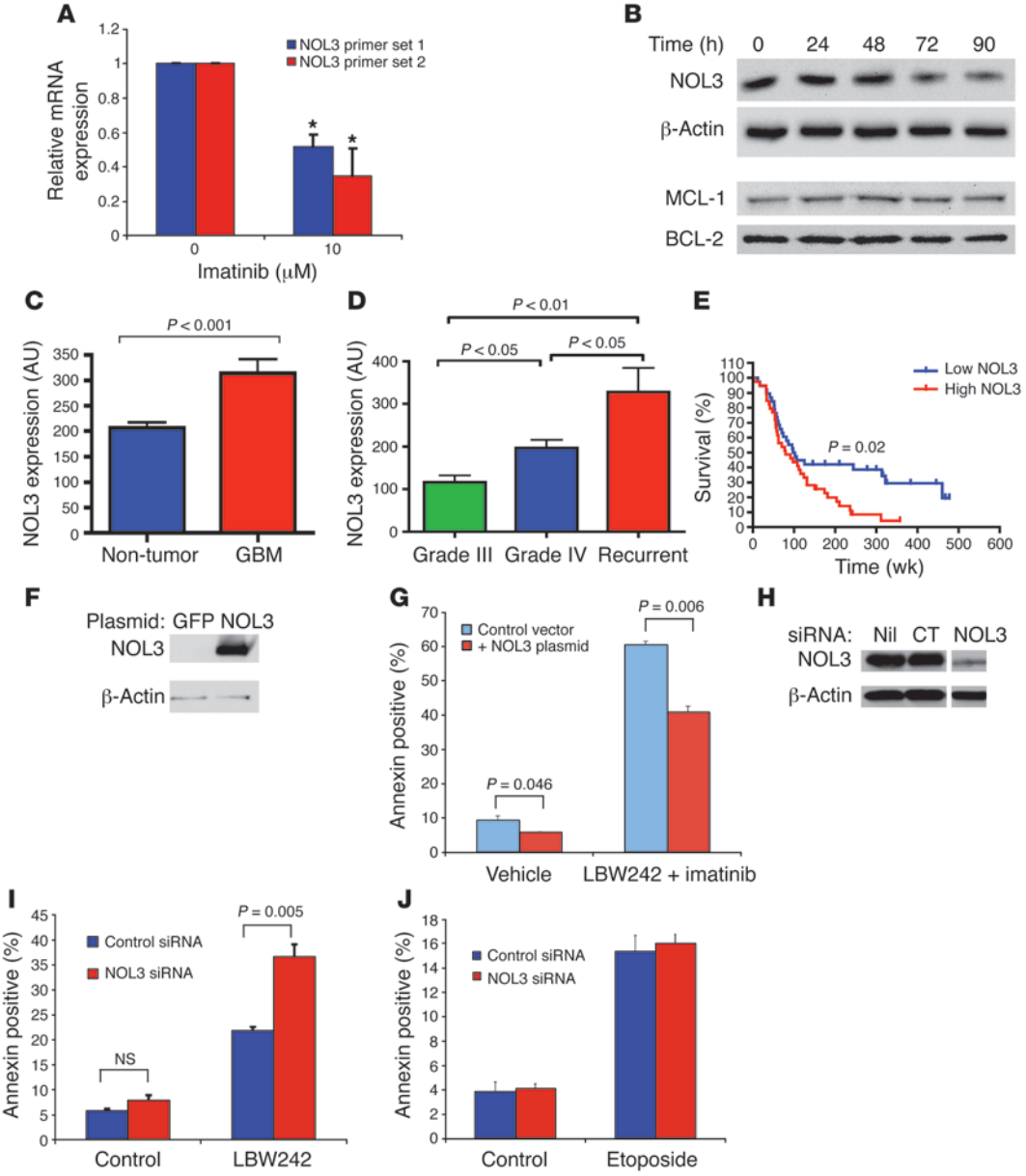


**Figure 5**

NOL3 is expressed in gliomas and is modulated by imatinib. (**A**) Quantitative RT-PCR evaluation of *NOL3* mRNA expression in LN827 cells following treatment with 10 μM imatinib. Data represent mean ± SEM of triplicates. *$P < 0.01$, 2-tailed Student's *t* test. (**B**) Western blot showing NOL3 protein levels in LN827 cells following treatment with imatinib 10 μM for the indicated times. (**C**) Comparison of *NOL3* mRNA expression levels in normal brain tissue, compared with GBM specimens. *P* values were calculated using unpaired *t* test with Welch's correction. Data values were obtained from the GSE4290 dataset (see Methods). (**D**) Comparison of *NOL3* mRNA expression levels in grade III, grade IV, and recurrent high-grade gliomas, with *P* values calculated using the 1-way ANOVA test. Data values were obtained from the GSE4271 dataset (see Methods). (**E**) Kaplan-Meier survival curves for patients with high-grade gliomas based on NOL3 expression level. Results were separated above or below the median NOL3 level, and *P* values were calculated by the log-rank test. Data values were obtained from the GSE4271 dataset. (**F**) Western blot showing NOL3 protein levels in 293T cells following transfection with NOL3 plasmid. (**G**) LN827 cells were transfected with CD19 plasmid and either NOL3 plasmid or control vector. Cells were then treated with LBW242 50 μM plus imatinib 10 μM or with vehicle control for 72 hours. Cells were stained with annexin V–PE and CD19-FITC antibodies and analyzed by flow cytometry, with CD19 used as a marker of successful transfection and annexin V–PE as a marker of apoptosis. *P* values were calculated by 2-tailed Student's *t* test. (**H**) LN827 cells were transfected with 50 nM NOL3 siRNA, control (CT) siRNA, or Lipofectamine 2000 only (Nil). Western blot was performed for NOL3 protein after 72 hours, with all samples on a single gel but not in contiguous wells. (**I**) LN827 cells were transfected with either control or NOL3 siRNA. LBW242 50 μM was added 5 hours after transfection. Apoptosis was determined by annexin V and PI staining after 72 hours of treatment. (**J**) LN827 cells were similarly treated with etoposide 50 μg/ml for 48 hours. *P* values were calculated using the 2-tailed Student's *t* test.

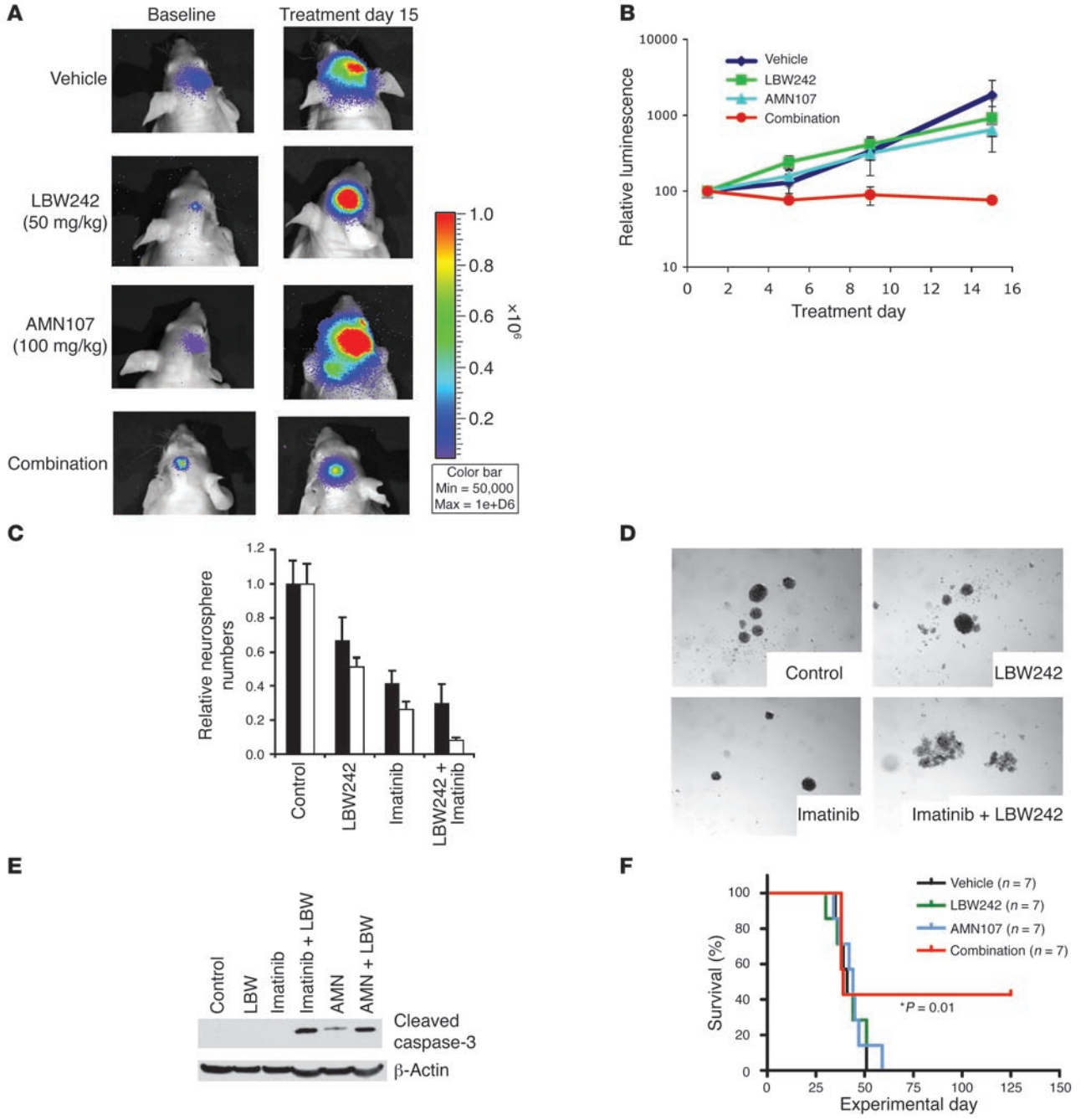


**Figure 6**

AMN107 and LBW242 combine to inhibit the growth of intracranial LN827 orthografts and primary human glioblastoma neurospheres in vitro and in vivo. (**A**) Bioluminescent images from control and treated animals at the start and end of a 15-day treatment with the indicated doses of LBW242 and/or AMN107. (**B**) Tumor burden was assessed by serial bioluminescence imaging and expressed relative to the start of treatment. Data are mean values ± SEM, $n = 6$ animals per group. (**C**) Primary human glioma neurospheres were derived from 2 different patients (BT69, white bars; BT79, black bars) and were treated with imatinib and/or LBW242. (**D**) Total neurosphere numbers were counted and photographed 10 days after plating, with data expressed as relative mean ± SD of triplicates. (**E**) Tumor neurospheres treated for 72 hours with imatinib, AMN107 (AMN), and/or LBW242 (LBW) were lysed and activated caspase-3 was assessed by immunoblot. (**F**) Kaplan-Meier survival curves for mice implanted with primary human glioma orthografts. Mice were treated for 12 consecutive days with vehicle, AMN107, LBW242, or a combination of AMN107 and LBW242, with treatments beginning 12 days after implant. *$P = 0.01$, combination versus all other groups, for experimental day 60 and all time points thereafter.

**Table 1**
Combinatorial index for treatment with LBW242 plus imatinib in glioma cells

| Cells | Expected survival proportion | Observed survival proportion | Combinatorial index |
|---|---|---|---|
| Primary hBT69 | 0.065 | 0.07 | 1.07 (additive) |
| Primary hBT74 | 0.306 | 0.147 | 0.48 (synergy) |
| Primary hBT78 | 0.18 | 0.29 | 1.61 (antagonism) |
| Primary hBT79 | 0.16 | 0.08 | 0.59 (synergy) |
| Primary hBT85 | 0.29 | 0.121 | 0.41 (synergy) |
| LN827 | 0.88 | 0.06 | 0.07 (synergy) |
| U87 | 1.08 | 0.63 | 0.58 (synergy) |

The combinatorial indices for LBW242 and imatinib were expressed as the ratio of observed/expected cells surviving, where the expected result was calculated as the proportion of surviving cells following treatment with LBW242 alone multiplied by the proportion of cells following treatment with imatinib alone.

ly expressed in normal cardiac, skeletal, and neurological tissue (44, 45). An independent quantitative RT-PCR analysis confirmed that imatinib significantly reduced *NOL3* mRNA expression (Figure 5A). Western blot confirmed that the reduction in NOL3 transcription over time led to a correlative decrease in NOL3 protein levels, but not of other antiapoptotic proteins (Figure 5B).

A role for NOL3 in gliomas has not to our knowledge been previously described. To determine the clinical relevance of NOL3 in malignant gliomas, we evaluated the expression of NOL3 utilizing previously published mRNA expression data (46, 47). We found that NOL3 was significantly overexpressed in malignant gliomas when compared with non-tumor brain tissue (Figure 5C). Evaluation of NOL3 expression in subsets of malignant glioma specimens revealed increasing expression with worsening grade of tumor (Figure 5D). Similarly, high expression of NOL3 in tumor specimens correlated with inferior patient survival (Figure 5E).

We next investigated whether modulating NOL3 expression had an impact on the observed synergy between imatinib and LBW242. First we ectopically expressed NOL3 in LN827 cells (Figure 5F) and assessed the effects on the induction of apoptosis by the combination of imatinib and LBW242. Transfection with NOL3 led to a marginal decrease in basal levels of apoptosis but had a far more significant impact on the proapoptotic effects of treatment with LBW242 and imatinib, with a 30% reduction in the number of cells undergoing apoptosis when compared with control cells (Figure 5G). Conversely, to test the antiapoptotic effects of NOL3, we assessed whether decreasing NOL3 expression alone was sufficient to sensitize cells to LBW242. siRNA knockdown of NOL3 led to decreased protein abundance (Figure 5H). While NOL3 depletion alone did not significantly increase apoptosis (Figure 5I), depletion of NOL3 combined with LBW242 resulted in a significant increase in cellular apoptosis (Figure 5I). In contrast, NOL3 depletion had no effect on the induction of apoptosis by etoposide (Figure 5J). Taken together, these results show that NOL3 expression is associated with glioma progression in patients, that ectopic expression of NOL3 can exert antiapoptotic effects in glioma cells, and that decreased expression may contribute to the proapoptotic effects of imatinib treatment. Since modulation of NOL3 expression only partially reverses the effects of imatinib and LBW242, it is likely that other effectors of apoptosis are important for mediating the full effects of this combination.

*PDGFR inhibition synergizes with IAP inhibition to suppress glioma growth in vivo and in primary human glioma neurospheres.* To extend these findings in vivo, we next tested the combination of growth factor inhibition and IAP inhibition in an orthotopic glioma model. LN827 cells were stereotactically implanted into the brains of mice. Tumor burden was serially assessed by bioluminescence imaging, which has previously been shown to be highly correlated with tumor volume (48, 49). Animals with established tumors, characterized by logarithmically increasing tumor burden, were divided into treatment cohorts. One group was treated with AMN107 at 100 mg/kg/d by oral gavage, one group with LBW242 at 50 mg/kg twice a day by oral gavage, one group with vehicle, and one group with the combination of LBW242 and AMN107. AMN107 was used in these studies due to its improved pharmacokinetic properties in mice in comparison with imatinib ($t_{1/2}$ < 2 h). Consistent with the in vitro studies, monotherapy with either AMN107 or LBW242 alone had no appreciable effect on tumor growth. In contrast, animals treated with both AMN107 and LBW242 had complete cessation of tumor growth (Figure 6, A and B). These results establish that combined inhibition of PDGFR and IAP produces synergistic antitumor efficacy in vivo in an orthotopic cell line glioma model.

Animals treated with LBW242 had no significant changes in weight (data not shown), suggesting no overt systemic toxicity. To further assess toxicity, animals treated with LBW242 for 2 weeks underwent full necropsy. Systematic evaluation of all major organ systems revealed no histological changes indicative of drug toxicity, including brain (contralateral to tumor implants), eyes, thyroid, lungs, liver, spleen, gastrointestinal tract, kidneys, adrenal gland, heart, striated muscle, bone, bone marrow, or vasculature.

Since it has been suggested that xenografts grown from traditional adherent serum cultured cell lines may be poor predictors of clinical outcome (50), we next examined this treatment combination in primary human glioma tumor neurospheres (51). In neurospheres derived from 2 different patients with GBM, LBW242 and imatinib had stand-alone activity, and in combination they had additive effects in decreasing overall neurosphere numbers (Figure 6C). To further confirm this finding, we calculated the combinatorial index of imatinib plus LBW242 in a total of 5 neurosphere cultures and 2 adherent cell lines. The effect was additive or synergistic in all but one of the cell cultures tested (Table 1). The morphological appearance of some neurospheres treated with LBW242 in combination with imatinib suggested aggregates of dead cells (Figure 6D). To specifically assess induction of apoptosis within these neurospheres, lysates from treated neurospheres were analyzed with an antibody specific for the activated form of caspase-3. Consistent with the data derived from glioma cell lines, there was no appreciable caspase-3 activation by imatinib or LBW242 alone, and minimal activation by AMN107 alone (Figure 6E). However, marked activation of caspase-3 was apparent when either imatinib or AMN107 was combined with LBW242 (Figure 6E).

To determine whether the same synergistic effect on primary glioma neurospheres could be recapitulated in the in vivo setting, we orthotopically implanted stem cell–enriched neurosphere cultures of primary human glioma cells intracranially in nude mice. After establishing tumors for 12 days, animals were divided into cohorts that were treated with vehicle, AMN107, LBW242, or a combination of AMN107 and LBW242, as described above. All animals treated with either vehicle or single agents died within 60 days. However, 3 of 7 mice treated in the combination arm

remained alive and well at 125 days follow-up, with no evidence of either disease or treatment toxicity (Figure 6F). The survival benefit at 60 days or more was highly statistically significant ($P = 0.01$, 2-tailed Fisher's exact test). Taken together, these results support the synergistic activity of PDGFR and IAP inhibition in both in vitro and in vivo models derived from glioma cell lines and primary human glioblastoma samples.

## Discussion

Novel therapies for malignant gliomas are desperately needed. In this study, we demonstrate that RTK inhibitors activate the apoptotic cascade, including induction of MOMP, but that downstream antiapoptotic mechanisms prevent caspase activation and apoptosis. Combination treatment with the small molecule IAP inhibitor LBW242 and inhibition of PDGFR resulted in synergistic induction of apoptosis and suppressed tumor growth in vitro, in vivo, and in primary glioma neurosphere models. Furthermore, the IAP inhibitor LBW242 was effectively combined with inhibitors that target the other growth factor RTKs, EGFR and IGF-1R. Thus, resistance to RTK inhibitors was overcome by concomitant inhibition of the IAPs.

These results have several potential implications. First, our results represent what we believe to be a novel approach to improve therapy with growth factor receptor inhibitors. While tyrosine kinase inhibitors hold great promise for improving outcomes, it is unlikely that a single targeted therapy will ever form a definitive therapy in malignant gliomas, which are characterized by multiple altered tumorigenic pathways alongside widespread inter- and intratumoral heterogeneity. Despite the importance of growth factor pathways in glioma tumorigenesis, clinical responses to growth factor receptor inhibitors in glioma patients have been limited and, when present, often transient. Unlike chronic myelogenous leukemia, for example, which is primarily driven by a single dominant oncogene and can effectively be treated by targeting that defect alone, in gliomas, targeted therapies and indeed conventional therapies are confounded by the multitude of abnormalities that act to thwart treatment efficacy.

We have shown that an alteration in the apoptotic pathway reduces the effect of treatments targeting the growth factor pathways. That is, PDGFR inhibition alone results in activation of the intrinsic pathway and mitochondrial permeabilization but does not cause caspase activation or apoptosis, indicating the presence of a downstream block in the apoptotic cascade. It is only following the addition of IAP inhibition that an increase in caspase activity results, with subsequent apoptosis and an enhanced antitumor effect seen both in vitro and in vivo. Thus the strategy of targeting 2 separate molecular pathways — the aberrantly expressed IAPs in combination with the highly dysregulated growth factor pathway — effectively suppresses tumor growth. Several recent reports have emerged that suggest that different SMAC mimetics can stimulate TNF production and propagate apoptosis via the extrinsic apoptotic pathway in certain tumor types (38–40). Notably, this led to the ability of SMAC mimetics to induce cell death as single agents in some cell lines. In our experiments LBW242 had no effect as a monotherapy and did not stimulate the extrinsic pathway, as assessed by measurement of caspase-8 activity. Therefore, while the mechanism of apoptosis was limited to the intrinsic pathway in this study, therapeutic application of IAP inhibitors may result in antitumor efficacy through pleiotropic mechanisms.

Second, our results suggest that multiple factors need to be considered when evaluating responsiveness to growth factor receptor inhibitors. To date, most analyses have focused on receptor mutations and molecular pathways directly related to receptor signaling, such as PTEN status. For example, it has been shown that a clinical response to EGFR inhibition is more likely in tumors that express the EGFRvIII mutant in association with an intact PTEN signaling pathway (4). However, other studies have shown conflicting findings — in 1 report the response was associated with EGFR amplification and expression but not EGFRvIII (52). Our results suggest that distant downstream regulatory mechanisms may be just as important in determining response to therapy both in the laboratory and in the clinic. Indeed, the IAPs represent one of the most downstream blockades to apoptosis, and their successful inhibition illustrates the fact that targeting more distal pathways in combination with RTKs may be at least as beneficial as focusing purely on upstream signaling proteins. Moreover, our results demonstrate what is to our knowledge a novel mechanism of bypassing molecular impediments to effective treatment. The synergy demonstrated appears to occur independent of, and without modulation of, Akt status. Both cell lines tested have mutations in the PTEN tumor suppressor gene (21), a factor not only associated with poor responses to growth factor receptor inhibitors, but also with an overall poor prognosis (46). By targeting the distal IAPs in combination with growth factor receptor inhibition, we have demonstrated a successful mechanism of bypassing the molecular PTEN/Akt blockade. Furthermore, the poor clinical responses seen with imatinib in glioma patient clinical trials has led to speculation that the lack of activity is due to poor penetration of the BBB. Our results offer an alternative explanation, that the RTK target is being inhibited but that antiapoptotic mechanisms confer resistance to cell death, as they do in conventional chemotherapy and radiotherapy.

Third, we have identified a potential role for the antiapoptotic protein NOL3 in glioma biology. NOL3 has been described to be present in normal heart, skeletal muscle, and brain tissue and has been shown to inhibit both the intrinsic and extrinsic apoptotic pathways (44, 45, 53). It acts to block the caspase activity of caspase-2 and -8 (44) but has also been shown to regulate the release of cytochrome *c* from the mitochondria by interfering with Bax activation (53). NOL3 has only recently been demonstrated to be expressed in various cancer cell lines (54) and to confer both chemo- and radioresistance in breast cancer cells (55). Here we found, in a retrospective analysis, that NOL3 was overexpressed in malignant gliomas when compared with normal brain tissue, with progressively higher levels of expression detected in worsening grades of tumor. High levels of expression correlated with poor prognosis and significantly inferior patient survival (Figure 5E). Prospective evaluation is needed to validate NOL3 as a prognostic indicator in gliomas. We have shown that PDGFR inhibition with imatinib leads to decreased abundance of NOL3 and that this effect may play a role in triggering the apoptotic pathway and thus sensitizing cells to IAP inhibition.

Fourth, the results here raise the prospect that similar combinatorial strategies may be relevant in other tumors. A subset of ovarian cancer has been shown to over express PDGFR and to respond to treatment with imatinib (56). However, as with gliomas, imatinib monotherapy is unable to induce apoptosis in ovarian cancers, and no efficacy has been demonstrated in clinical trials (56, 57). Similarly, while imatinib has demonstrated efficacy in small

cell lung cancers, no induction of apoptosis has been observed (58). Our results raise the prospect that a similar combinatorial strategy may be adopted to improve the response to PDGFR inhibition in cancers other than glioma. Moreover, the same may be applied to other RTK inhibitors in a variety of cancers. For example, for unknown reasons, tumor EGFR status does not predict the response of colorectal cancers to EGFR inhibitors (59). Extrapolation of our results suggests that antiapoptotic proteins may be an important biomarker predictive of response to treatment with RTK inhibitors and that targeting the apoptotic pathway in conjunction with RTK inhibition may have the potential to further improve tumor responses.

Finally, this represents what we believe to be the first reported approach to targeting IAPs in gliomas that offers a feasible path for translation to the clinic. Previous preclinical studies validating IAPs as therapeutic targets in gliomas have utilized peptides, which in some cases were administered by direct intratumoral injection (26, 31, 32). While these innovative reports validated the notion of targeting IAPs, in terms of clinical translation, it is not feasible to use the peptides employed due to their instability and poor cellular permeability (60). The development of small molecule inhibitors of IAPs provides a more tractable method for clinical translation. A small molecule Smac mimetic was previously shown to have synergistic effects when administered in vitro in combination with TRAIL in a glioma cell line, but was not tested in vivo (27, 28). Our results establish the preclinical rationale for clinical testing of small molecule IAP inhibitors in combination with RTK inhibitors in patients with gliomas.

## Methods

*Cell culture*. The human glioma cell lines U87 and LN827 were cultured in DMEM complete medium supplemented with 10% heat-inactivated fetal calf serum, penicillin (100 U/ml) and streptomycin (100 μg/ml). Cells were cultured in a humidified 10% $CO_2$ atmosphere at 37°C and maintained in a logarithmic growth phase for all experiments.

*Drugs*. LBW242, imatinib, AMN107, AEW541, and PKI166 were generously provided by Novartis Pharma. Triciribine was purchased from Calbiochem. Stock solutions of LBW242, AMN107, AEW541, PKI166, and triciribine were dissolved in DMSO (Sigma-Aldrich) and stored at –20°C. Imatinib stock was dissolved in double-distilled water and stored at –20°C. All drugs were diluted in fresh medium immediately prior to use.

*Time-resolved fluorescence resonance energy transfer*. GST-XIAP-BIR3 (plasmid gift of Yigong Shi, Princeton University, Princeton, New Jersey, USA) was preincubated with LBW242 at varying concentrations in a 96-well format for 30 minutes. APC-labeled anti-GST antibody (PerkinElmer), europium-labeled streptavidin beads (PerkinElmer), and biotin-Smac were then added. Each well contained a final concentration of 6.25 nM GST-XIAP-BIR3 with 3.5 nM biotin-Smac, 1 nM Eu-streptavidin, and 25 nM anti–GST-APC in the presence or absence of LBW242 at varying concentrations. Plates were incubated for a further 30 minutes and fluorescence read using an Envision multilabel reader (PerkinElmer; emission filters: europium 615 nM, APC 665 nM, and optical module Lance Eu/APC Dual 452). The $IC_{50}$ at which 50% of GST-BIR3 is released from biotinylated Smac were determined using the XL-fit4 program (IDBS Software).

*Cell-free caspase assay*. A cell-free extract was prepared as described previously (61). In brief, 100 μg of 293T cell extract (8 mg/ml) was mixed with cytochrome *c* (Sigma-Aldrich) and dATP (Gibco BRL) in a 96-well plate format. Recombinant GST-XIAP-BIR3 fusion protein was added with or without LBW242 at the dosages indicated in Figure 1C. Hypotonic lysis buffer was added to bring the final volume to 25 μl. The contents were mixed and the plate incubated at 30°C for 30 minutes to activate the extract. A cocktail of 7 μl Ac-DEVD-AMC (BD Biosciences) caspase-3 substrate, 20 μl 5× apoptosis buffer, and 48 μl di$H_2O$ was then added, plates incubated for a further 30 minutes at 30°C, and fluorescence read at 360/460 nm on Cytofluor II.

*Measurement of LBW242 concentrations in vivo*. Athymic nude (*nu/nu*) mice subcutaneously implanted with SK-OV-3 xenograft were administered i.v. a 50-mg/kg dose of LBW242 or vehicle control once daily for 14 days. Four hours after the last dose, animals from control and treated groups were sacrificed and tissues and blood samples collected. For quantitative analysis of LBW242, individual tumor samples were added with 5 parts (weight/volume) of PBS (pH 7.4) and homogenized (Autogizer; Tomtec) at room temperature. Blood samples were treated with sodium EDTA anticoagulant and further centrifuged to obtain plasma.

Blank plasma or tissue homogenates from animals untreated with either vehicle or test compound were used to prepare calibration standards from 0.5 to 500 μM of LBW242 by a serial dilution method. Fifty microliters of plasma or tissue homogenate calibration standards and study samples were successively added with 25 μl of 2 μM glyburide internal standard solution and 0.4 ml of protein precipitation solvent mixture (acetonitrile/ethanol/acetic acid, 90:10:0.2, vol/vol), thoroughly vortexed for 3 minutes, and centrifuged (1,500 *g*) for 5 minutes. A 100-μl aliquot of clear supernatant was transferred into a 96-well plate and 50 μl of 0.1% acetic acid was added and mixed well, and a 10-μl portion of the resulting solution was injected onto a HPLC/MS/MS system for quantitative analysis of LBW242. A C-18 reverse-phase HPLC column (Ace3 C18; 3.0 × 50 mm; 3.5-μm particle size; Mac Mod Analytical Inc.) eluted with a gradient mobile phase (solvent A, 0.1% formic acid in water; solvent B, 0.1% formic acid in acetonitrile) chromatographically separated LBW242 and internal standard from endogenous materials. The effluent mobile phase was introduced into a tandem mass spectrometry detector (API 4000; Applied Biosciences) to monitor LBW242 and internal standard via electrospray-positive ionization, multiple reaction monitoring mode. Calibration curves (0.5 to 500 μM concentration range) of LBW242 in plasma or tumor using peak area ratio of compound to internal standard generated with quadratic regression fit (Analyst software, version 4; Applied Biosystems) were used for quantification of test compound concentrations.

*Cellular proliferation assays*. Cell proliferation assays were performed with CellTiter 96 Aqueous One Solution Cell Proliferation Assay (Promega) as per the manufacturer's recommendations. Briefly, $1 \times 10^3$ cells were plated in 100 μl of medium in 96-well microtiter plates and incubated for 24 hours. The concentrations of inhibitors (indicated in Figure 1H, Figure 2, and Figure 4B) were added and the cells incubated for a further 48 to 72 hours. Labeling reagent (20 μl) was added to each well and allowed to incubate at 37°C for 2 hours. The absorbance was then read at 490 nm with a 96-well plate reader.

*Caspase-3/7 activity and caspase-8 activity assays*. Caspase-3/7 activity was measured with the Apo-One Homogenous Caspase-3/7 Assay kit (Promega) according to the manufacturer's protocol. Briefly, $1 \times 10^3$ cells in 100 microliters of medium were plated in 96-well microtiter plates and incubated for 24 hours. The indicated concentration of inhibitors was added and the cells incubated for a further 48 hours. Labeling reagent (100 μl) was added to each well. Caspase-3/7 activity was measured after 6 hours' incubation on a fluorescence plate reader, with an excitation wavelength of 485 nm and emission wavelength of 535 nm. Caspase-8 activity was measured with the Caspase-Glo 8 assay (Promega) according to the manufacturer's protocol. Cells were prepared as above, 100 μl of labeling reagent was added to each well, and luminescence was measured after 2 hours of incubation on a plate-reading luminometer.

*Flow cytometric and annexin V analysis*. Cells ($2.5 \times 10^5$) were plated in 60-mm plates in 2 ml of medium and cultured for 24 hours. The medium was removed and inhibitors were added in DMEM with 1% serum. Cells were

cultured for a further 72 hours, collected for analysis, washed twice in cold PBS, and resuspended in 100 μl of binding buffer containing an annexin V–FITC and propidium iodide mixture (Invitrogen) as per the manufacturer's instructions. Before FACS analysis, an additional 400 μl of binding buffer was added to the cell suspension. FACS analysis was performed on FACScan and gated to exclude cellular debris; 10,000 events were collected for each sample.

*Antibodies and western blotting.* Cells were pretreated with inhibitors; washed twice in ice-cold PBS; lysed with RIPA buffer (Boston Bioproducts) containing 50 mM Tris-Cl (pH 7.4), 150 mM NaCl, 1% NP-40, 0.5% sodium deoxycholate, and 0.1% SDS with added 1 mM EDTA, 1 mM sodium orthovanadate, 50 mM NaF, and Complete Protease Inhibitor cocktail (Roche Applied Science); vortexed for 5 seconds; and centrifuged at 16,100 *g* for 10 minutes at 4°C. Equal amounts of protein were loaded onto 4%–12% Bis-Tris-polyacrylamide gel (Invitrogen), separated by electrophoresis, and transferred to nitrocellulose membranes (Invitrogen). Western blots were probed with β-actin (Sigma-Aldrich), PDGFR-β antibody (Abcam), and phospho–PDGFR-β antibody, phospho-Akt, Bad, phospho-Bad Ser112 and Ser136, MCL-1, BCL2 (all from Cell Signaling), and NOL3 C-Terminus (Chemicon) as per the manufacturer's instructions. Blots were then labeled with anti-rabbit or anti-mouse IgG-HRP antibody (Vector Laboratories) and visualized using an enhanced chemiluminescence system (Amersham) or electronic chemiluminescence (ChemiDoc XRS System; Bio Rad).

*Immunoprecipitation studies.* For PDGFR immunoprecipitation, $5 \times 10^5$ cells were plated in 2 ml of medium in 60-mm plates and incubated overnight. Medium was removed and the cells serum starved for 24 hours. Inhibitors were added for 90 minutes and the cells then stimulated with serum for 5 minutes. Cells were washed twice with ice-cold PBS and lysed with RIPA buffer (Boston Bioproducts) containing 50 mM Tris-Cl (pH 7.4), 150 mM NaCl, 1% NP-40, 0.5% sodium deoxycholate, and 0.1% SDS with added 1 mM EDTA, 1 mM sodium orthovanadate, 50 mM NaF, and Complete Protease Inhibitor cocktail (Roche Applied Science). Standardized aliquots of lysate were incubated with PDGF-β receptor antibody (Abcam) overnight at 4°C and immobilized on Protein G Sepharose (Amersham Biosciences) for 1 hour. Beads were washed extensively with buffer. Samples were fractionated on SDS-PAGE, transferred to nitrocellulose, and immunoblotted with phospho–PDGFR-β antibody (Cell Signaling) and PDGFR-β antibody (Abcam) as described above.

For caspase-9 immunoprecipitation, LN827 cells were treated with LBW242 or DMSO control for 4 hours. For each concentration of LBW242, dishes (4 × 15 cm) were scraped into ice-cold lysis buffer (150 mM NaCl, 1% Triton-X, 50 μM Tris-Cl (pH 8.0), 1 mM EDTA) with Complete Protease Inhibitor cocktail. Protein concentration was determined by Bradford Assay (BioRad), and 50 μg of each lysate was removed as the input. Anti–caspase-9 antibody (BD Biosciences) was bound overnight at 4°C and then immobilized on Protein G Sepharose for 1 hour. Beads were extensively washed with lysis buffer, fractionated and transferred to nitrocellulose as described above, and immunoblotted with XIAP (Cell Signaling), and caspase-9 (Cell Signaling) antibodies. Image analysis was performed using ImageJ (NIH) and expressed relative to DMSO controls.

*Mitochondrial permeabilization analysis.* Cells ($5 \times 10^5$) were seeded in each 6-cm plate and treated with drugs as indicated in Figure 3A. Following 48 hours of incubation, cells were collected and the mitochondria separated from cytoplasm using a mitochondria isolation kit (Pierce Biotechnology) as per the manufacturer's instructions. The cytosolic fraction was collected, and equal amounts of protein were fractionated on SDS-PAGE, transferred to nitrocellulose, and immunoblotted with cytochrome *c* antibody (BD Biosciences — Pharmingen), Smac/DIABLO antibody (Cell Signaling), and β-actin antibody (Sigma-Aldrich) as described above.

*Microarray analysis.* LN827 cells ($1 \times 10^5$) were plated in 6-cm plates and treated with imatinib 10 μM in DMEM plus 1% serum for 36 hours. Following treatment, cells were harvested and RNA extracted using RNeasy Mini kit (Qiagen), as per the manufacturer's instructions. Gene expression profiling of the apoptotic pathway was performed and analyzed using RT$^2$ Profiler PCR Array Human Apoptosis, catalog no. APHS-012B (SuperArray Bioscience), as per the manufacturer's instructions.

*Real-time PCR.* LN827 cells were treated in triplicate with imatinib 10 μM or vehicle control for 15 hours, harvested, and homogenized using QIAshredder columns (Qiagen), and total RNA was extracted using RNeasy Mini kit (Qiagen) according to the manufacturer's protocol. Real-time PCR was then conducted using 5 μg of RNA added to 10 U of Superscript III reverse transcriptase (Invitrogen), 5 μM forward and reverse primers, and 1× SYBR Green (Qiagen). Reactions were run and analyzed using the Stratagene Mx3000p instrument and software (Stratagene).

*Gene expression analysis.* Normalized gene expression data was obtained from the Gene Expression Omnibus online datasets GSE4290 (http://www.ncbi.nlm.nih.gov/geo/query/acc.cgi?acc=GSE4290) and GSE4271 (http://www.ncbi.nlm.nih.gov/geo/query/acc.cgi?acc=GSE4271), and NOL3 expression levels were analyzed using GraphPad Prism 4 software (Figure 5E).

*Plasmid transfection.* NOL3 plasmid (NM_003946; Origene) was tested in 293T cells after transfection using Lipofectamine 2000 (Invitrogen). Cells were harvested after 24 hours and subjected to western blot for NOL3 protein. LN827 cells ($1 \times 10^5$ per well of a 6-well plate) were cultured overnight, then treated with the transfection reagent Fugene 6 (Roche Applied Science) with 3.2 μg of either NOL3 plasmid or pcDNA3.1-HisC control vector, plus 0.8 μg of CD19 plasmid per well as an internal control for transfection efficiency. After 6 hours the incubation medium was replaced and cells were incubated overnight. The following day the medium was replaced with DMEM plus 1% serum, and cells were treated with LBW242 and imatinib or vehicle control as indicated in Figure 5G. After a further 72 hours of incubation, cells were collected, stained with Annexin V–PE (BD Biosciences — Pharmingen) and CD19-FITC antibody, and analyzed by flow cytometry.

*siRNA knockdown.* LN827 cells were treated with Lipofectamine 2000 (Invitrogen) and transfected with pooled NOL3 siRNA (NM_003946; Dharmacon) or control siRNA (Dharmacon) for 5 hours as per the manufacturer's instructions. The medium was changed and replaced with DMEM and 1% serum plus imatinib 10 μM, LBW242 50 μM, and/or vehicle control, as indicated in Figure 5, I and J. After 72 hours of incubation, cells were collected and analyzed for apoptosis as described above.

*Tumor cell line xenografts.* Tumor cell lines were harvested in midlogarithmic growth phase and resuspended in PBS. Homozygous NCR nude mice (Charles River Laboratories) were anesthetized i.p. with ketamine hydrochloride at 150 mg/kg and xylazine at 12 mg/kg (Phoenix Pharmaceuticals). A small surgical incision along the midline was made to expose the calvarium, and the periosteum was removed with a sterile cotton swab. Mice were restrained in a stereotactic frame (Stoeltling), and a small burr-hole (size 34; Roboz) was created at 2 mm lateral and 2 mm posterior to the bregma. LN827-LN cells ($5 \times 10^5$) in 10 μl PBS were injected through a 27-gauge needle over 3 minutes (3.3 μl/min) at 3 mm below the dura. The incision was closed with wound clips (Becton Dickinson; catalog no. 427631) and removed 5–7 days after surgery.

Mice were imaged at least twice after implantation of cells to identify those in which tumor burden increased over time. Three weeks after implantation of LN827-LN cells, cohorts of 40 mice per experiment with approximately equivalent tumor bioluminescence were divided into equal control and treatment groups. Mice were treated with 50 mg/kg of LBW242 per oral (PO) once daily and/or 100 mg/kg of AMN107 PO daily for 14 days.

For in vivo imaging, mice were anesthetized, injected with D-luciferin at 50 mg/ml i.p. (Xenogen), and imaged with the IVIS Imaging System (Xenogen) for 10–120 s, bin size 2. To quantify bioluminescence, identical circular regions of interest were drawn to encircle the entire head of each animal, and the integrated flux of photons (photons per second) within each region of interest was determined by using the LIVING IMAGE software package (LI Version 2.50; Xenogen Corporation). Data were normalized to bioluminescence at the initiation of treatment for each animal. All animal studies were performed under protocols approved by the Dana-Farber Cancer Institute Animal Care and Use Committee.

*Glioma neurosphere assays*. Collection and use of fresh and discarded human tumor tissue was approved by the Brigham and Women's Hospital Institutional Review Board. After frozen section diagnosis of malignant glioma by the attending neuropathologist, tumor material was grossly dissected from the tissue sample. Portions of the tumors were collected in chilled media for the studies described here, and other portions were allocated for paraffin embedding for histological diagnosis and for genotyping. Expansion of tumor material and propagation was accomplished by subcutaneous implantation in NOD-SCID mice (cells were never grown on plastic or in FBS). When tumors reached approximately 1 cm in size, tumors were disaggregated and cells were counted and then reimplanted in mice or grown in serum-free media with EGF, FGF, and leukemia inhibitory factor, as described previously (51, 62) to form tumor neurospheres. Imatinib (5 μM) and LBW242 (50 μM) were added 24 hours after plating, and tumor neurospheres were counted 10 days after plating. The combinatorial indices for LBW242 and imatinib were expressed as the ratio of observed/expected cells surviving, where the expected result was calculated as the proportion of surviving cells following treatment with LBW242 alone multiplied by the proportion of cells following treatment with imatinib alone. For assessment of apoptosis, tumor neurospheres were preestablished for 7 days, imatinib and LBW242 were added, and tumor neurospheres were harvested 3 days later. Tumor neurospheres were lysed by resuspending in SDS-PAGE loading buffer and homogenized by centrifugation (Qiashredder; Qiagen). Immunoblot utilized a cleaved caspase-3 antibody (Cell Signaling).

For the in vivo experiments, hBT37 cells were resuspended in PBS at a concentration of 20,000 viable cells/5 μl PBS and injected into the right caudate as previously described (62). Twelve days following tumor implantation, mice were divided into 4 equal treatment groups and treated with vehicle, LBW242 (25 mg/kg i.p. daily), AMN107 (100 mg/kg PO daily), or a combination of LBW242 and AMN107. The treatments were administered for 12 days, following which the animals were monitored for survival. Animals were sacrificed at the onset of neurological symptoms or once moribund.

*Statistics*. Student's *t* test was calculated using Microsoft Excel. Log-rank test was calculated using GraphPad Prism. Fisher's exact test was calculated using SPSS. All *P* values are 2 tailed. *P* values less than 0.05 were considered significant.

## Acknowledgments

This work was supported by grants from the Dana-Farber Cancer Institute–Novartis Drug Discovery Program (to A.L. Kung), the Royal Australasian College of Physicians Rowden White Fellowship (to D.S. Ziegler), the Hagerty Fund Research Award (to D.S. Ziegler, S. Kesari, and A.L. Kung), the Leonard Florence Brain Tumor Fund (to S. Kesari), and the Australian-American Fulbright Commission (to D.S. Ziegler).

Received for publication October 2, 2007, and accepted in revised form June 18, 2008.

Address correspondence to: Andrew L. Kung, Department of Pediatric Oncology, Dana-Farber Cancer Institute, 44 Binney Street, Mayer 649, Boston, Massachusetts 02115, USA. Phone: (617) 632-5731; Fax: (617) 582-8096; E-mail: andrew_kung@dfci.harvard.edu.

David S. Ziegler's present address is: Centre for Children's Cancer and Blood Disorders, Sydney Children's Hospital and the Children's Cancer Institute Australia for Medical Research, Randwick, New South Wales, Australia.

1. DeAngelis, L.M. 2001. Brain tumors. *N. Engl. J. Med.* **344**:114–123.
2. Kitange, G.J., Templeton, K.L., and Jenkins, R.B. 2003. Recent advances in the molecular genetics of primary gliomas. *Curr. Opin. Oncol.* **15**:197–203.
3. Broniscer, A., and Gajjar, A. 2004. Supratentorial high-grade astrocytoma and diffuse brainstem glioma: two challenges for the pediatric oncologist. *Oncologist.* **9**:197–206.
4. Mellinghoff, I.K., et al. 2005. Molecular determinants of the response of glioblastomas to EGFR kinase inhibitors. *N. Engl. J. Med.* **353**:2012–2024.
5. Gammeltoft, S., Ballotti, R., Kowalski, A., Westermark, B., and Van Obberghen, E. 1988. Expression of two types of receptor for insulin-like growth factors in human malignant glioma. *Cancer Res.* **48**:1233–1237.
6. Kiaris, H., Schally, A.V., and Varga, J.L. 2000. Antagonists of growth hormone-releasing hormone inhibit the growth of U-87MG human glioblastoma in nude mice. *Neoplasia.* **2**:242–250.
7. Fleming, T.P., et al. 1992. Amplification and/or overexpression of platelet-derived growth factor receptors and epidermal growth factor receptor in human glial tumors. *Cancer Res.* **52**:4550–4553.
8. Hermanson, M., et al. 1992. Platelet-derived growth factor and its receptors in human glioma tissue: expression of messenger RNA and protein suggests the presence of autocrine and paracrine loops. *Cancer Res.* **52**:3213–3219.
9. Guha, A., Dashner, K., Black, P.M., Wagner, J.A., and Stiles, C.D. 1995. Expression of PDGF and PDGF receptors in human astrocytoma operation specimens supports the existence of an autocrine loop. *Int. J. Cancer.* **60**:168–173.
10. Kilic, T., et al. 2000. Intracranial inhibition of platelet-derived growth factor-mediated glioblastoma cell growth by an orally active kinase inhibitor of the 2-phenylaminopyrimidine class. *Cancer Res.* **60**:5143–5150.
11. Wen, P.Y., et al. 2006. Phase I/II study of imatinib mesylate for recurrent malignant gliomas: North American Brain Tumor Consortium Study 99–08. *Clin. Cancer Res.* **12**:4899–4907.
12. Rich, J.N., et al. 2004. Phase II trial of gefitinib in recurrent glioblastoma. *J. Clin. Oncol.* **22**:133–142.
13. Reardon, D.A., Rich, J.N., Friedman, H.S., and Bigner, D.D. 2006. Recent advances in the treatment of malignant astrocytoma. *J. Clin. Oncol.* **24**:1253–1265.
14. Camp, E.R., et al. 2005. Molecular mechanisms of resistance to therapies targeting the epidermal growth factor receptor. *Clin. Cancer Res.* **11**:397–405.
15. Chakravarti, A., Chakladar, A., Delaney, M.A., Latham, D.E., and Loeffler, J.S. 2002. The epidermal growth factor receptor pathway mediates resistance to sequential administration of radiation and chemotherapy in primary human glioblastoma cells in a RAS-dependent manner. *Cancer Res.* **62**:4307–4315.
16. Servidei, T., Riccardi, A., Sanguinetti, M., Dominici, C., and Riccardi, R. 2006. Increased sensitivity to the platelet-derived growth factor (PDGF) receptor inhibitor STI571 in chemoresistant glioma cells is associated with enhanced PDGF-BB-mediated signaling and STI571-induced Akt inactivation. *J. Cell. Physiol.* **208**:220–228.
17. Lefranc, F., Brotchi, J., and Kiss, R. 2005. Possible future issues in the treatment of glioblastomas: special emphasis on cell migration and the resistance of migrating glioblastoma cells to apoptosis. *J. Clin. Oncol.* **23**:2411–2422.
18. Ziegler, D.S., Kung, A.L., and Kieran, M.W. 2008. Anti-apoptosis mechanisms in malignant gliomas. *J. Clin. Oncol.* **26**:493–500.
19. Nakada, M., et al. 2007. Molecular targets of glioma invasion. *Cell. Mol. Life Sci.* **64**:458–478.
20. Bogler, O., and Mikkelsen, T. 2005. Angiogenesis and apoptosis in glioma: two arenas for promising new therapies. *J. Cell. Biochem.* **96**:16–24.
21. Ishii, N., et al. 1999. Frequent co-alterations of TP53, p16/CDKN2A, p14ARF, PTEN tumor suppressor genes in human glioma cell lines. *Brain Pathol.* **9**:469–479.
22. Steinbach, J.P., and Weller, M. 2004. Apoptosis in gliomas: molecular mechanisms and therapeutic implications. *J. Neurooncol.* **70**:247–256.
23. Wagenknecht, B., et al. 1999. Expression and biological activity of X-linked inhibitor of apoptosis (XIAP) in human malignant glioma. *Cell Death Differ.* **6**:370–376.
24. Chen, Z., et al. 1999. A human IAP-family gene, apollon, expressed in human brain cancer cells. *Biochem. Biophys. Res. Commun.* **264**:847–854.
25. Chakravarti, A., et al. 2002. Quantitatively determined survivin expression levels are of prognostic value in human gliomas. *J. Clin. Oncol.* **20**:1063–1068.
26. Fulda, S., Wick, W., Weller, M., and Debatin, K.M.

2002. Smac agonists sensitize for Apo2L/TRAIL- or anticancer drug-induced apoptosis and induce regression of malignant glioma in vivo. *Nat. Med.* **8**:808–815.
27. Li, L., et al. 2004. A small molecule Smac mimic potentiates TRAIL- and TNFalpha-mediated cell death. *Science.* **305**:1471–1474.
28. Roa, W.H., et al. 2003. X-linked inhibitor regulating TRAIL-induced apoptosis in chemoresistant human primary glioblastoma cells. *Clin. Invest. Med.* **26**:231–242.
29. Fesik, S.W. 2005. Promoting apoptosis as a strategy for cancer drug discovery. *Nat. Rev. Cancer.* **5**:876–885.
30. Chauhan, D., et al. 2007. Targeting mitochondrial factor Smac/DIABLO as therapy for multiple myeloma (MM). *Blood.* **109**:1220–1227.
31. Giagkousiklidis, S., et al. 2005. Sensitization for gamma-irradiation-induced apoptosis by second mitochondria-derived activator of caspase. *Cancer Res.* **65**:10502–10513.
32. Mizukawa, K., et al. 2006. Synthetic Smac peptide enhances the effect of etoposide-induced apoptosis in human glioblastoma cell lines. *J. Neurooncol.* **77**:247–255.
33. Arnt, C.R., Chiorean, M.V., Heldebrant, M.P., Gores, G.J., and Kaufmann, S.H. 2002. Synthetic Smac/DIABLO peptides enhance the effects of chemotherapeutic agents by binding XIAP and cIAP1 in situ. *J. Biol. Chem.* **277**:44236–44243.
34. Groothuis, D.R. 2000. The blood-brain and blood-tumor barriers: A review of strategies for increasing drug delivery. *Neuro. Oncol.* **2**:45–59.
35. Shamah, S.M., Stiles, C.D., and Guha, A. 1993. Dominant-negative mutants of platelet-derived growth factor revert the transformed phenotype of human astrocytoma cells. *Mol. Cell. Biol.* **13**:7203–7212.
36. Klein, S., McCormick, F., and Levitzki, A. 2005. Killing time for cancer cells. *Nat. Rev. Cancer.* **5**:573–580.
37. Weisberg, E., et al. 2005. Characterization of AMN107, a selective inhibitor of native and mutant Bcr-Abl. *Cancer Cell.* **7**:129–141.
38. Gaither, A., et al. 2007. A Smac mimetic rescue screen reveals roles for inhibitor of apoptosis proteins in tumor necrosis factor-alpha signaling. *Cancer Res.* **67**:11493–11498.
39. Vince, J.E., et al. 2007. IAP antagonists target cIAP1 to induce TNFalpha-dependent apoptosis. *Cell.* **131**:682–693.
40. Varfolomeev, E., et al. 2007. IAP antagonists induce autoubiquitination of c-IAPs, NF-kappaB activation, and TNFalpha-dependent apoptosis. *Cell.* **131**:669–681.
41. Garcia-Echeverria, C., et al. 2004. In vivo antitumor activity of NVP-AEW541-A novel, potent, and selective inhibitor of the IGF-IR kinase. *Cancer Cell.* **5**:231–239.
42. Bruns, C.J., et al. 2000. Blockade of the epidermal growth factor receptor signaling by a novel tyrosine kinase inhibitor leads to apoptosis of endothelial cells and therapy of human pancreatic carcinoma. *Cancer Res.* **60**:2926–2935.
43. Alikhani, M., Alikhani, Z., and Graves, D.T. 2005. FOXO1 functions as a master switch that regulates gene expression necessary for tumor necrosis factor-induced fibroblast apoptosis. *J. Biol. Chem.* **280**:12096–12102.
44. Koseki, T., Inohara, N., Chen, S., and Nunez, G. 1998. ARC, an inhibitor of apoptosis expressed in skeletal muscle and heart that interacts selectively with caspases. *Proc. Natl. Acad. Sci. U. S. A.* **95**:5156–5160.
45. Hong, Y.M., et al. 2003. Down-regulation of ARC contributes to vulnerability of hippocampal neurons to ischemia/hypoxia. *FEBS Lett.* **543**:170–173.
46. Phillips, H.S., et al. 2006. Molecular subclasses of high-grade glioma predict prognosis, delineate a pattern of disease progression, and resemble stages in neurogenesis. *Cancer Cell.* **9**:157–173.
47. Sun, L., et al. 2006. Neuronal and glioma-derived stem cell factor induces angiogenesis within the brain. *Cancer Cell.* **9**:287–300.
48. Rubin, J.B., et al. 2003. A small-molecule antagonist of CXCR4 inhibits intracranial growth of primary brain tumors. *Proc. Natl. Acad. Sci. U. S. A.* **100**:13513–13518.
49. Szentirmai, O., et al. 2006. Noninvasive bioluminescence imaging of luciferase expressing intracranial U87 xenografts: correlation with magnetic resonance imaging determined tumor volume and longitudinal use in assessing tumor growth and antiangiogenic treatment effect. *Neurosurgery.* **58**:365–372.
50. Kung, A.L. 2007. Practices and pitfalls of mouse cancer models in drug discovery. *Adv. Cancer Res.* **96**:191–212.
51. Singh, S.K., et al. 2004. Identification of human brain tumour initiating cells. *Nature.* **432**:396–401.
52. Haas-Kogan, D.A., et al. 2005. Epidermal growth factor receptor, protein kinase B/Akt, and glioma response to erlotinib. *J. Natl. Cancer Inst.* **97**:880–887.
53. Gustafsson, A.B., Tsai, J.G., Logue, S.E., Crow, M.T., and Gottlieb, R.A. 2004. Apoptosis repressor with caspase recruitment domain protects against cell death by interfering with Bax activation. *J. Biol. Chem.* **279**:21233–21238.
54. Wang, M., Qanungo, S., Crow, M.T., Watanabe, M., and Nieminen, A.L. 2005. Apoptosis repressor with caspase recruitment domain (ARC) is expressed in cancer cells and localizes to nuclei. *FEBS Lett.* **579**:2411–2415.
55. Mercier, I., et al. 2005. ARC, an apoptosis suppressor limited to terminally differentiated cells, is induced in human breast cancer and confers chemo- and radiation-resistance. *Cell Death Differ.* **12**:682–686.
56. Matei, D., Chang, D.D., and Jeng, M.H. 2004. Imatinib mesylate (Gleevec) inhibits ovarian cancer cell growth through a mechanism dependent on platelet-derived growth factor receptor alpha and Akt inactivation. *Clin. Cancer Res.* **10**:681–690.
57. Coleman, R.L., et al. 2006. Phase II trial of imatinib mesylate in patients with recurrent platinum- and taxane-resistant epithelial ovarian and primary peritoneal cancers. *Gynecol. Oncol.* **101**:126–131.
58. Krystal, G.W., Honsawek, S., Litz, J., and Buchdunger, E. 2000. The selective tyrosine kinase inhibitor STI571 inhibits small cell lung cancer growth. *Clin. Cancer Res.* **6**:3319–3326.
59. Hoff, P.M., and Ellis, L.M. 2007. Targeted therapy trials: approval strategies, target validation, or helping patients? *J. Clin. Oncol.* **25**:1639–1641.
60. Wright, C.W., and Duckett, C.S. 2005. Reawakening the cellular death program in neoplasia through the therapeutic blockade of IAP function. *J. Clin. Invest.* **115**:2673–2678.
61. Deveraux, Q.L., Welsh, K., and Reed, J.C. 2000. Purification and use of recombinant inhibitor of apoptosis proteins as caspase inhibitors. *Methods Enzymol.* **322**:154–161.
62. Ligon, K.L., et al. 2007. Olig2-regulated lineage-restricted pathway controls replication competence in neural stem cells and malignant glioma. *Neuron.* **53**:503–517.